Edelweiss Applied Science and Technology
ISSN: 2576-8484
Vol. 8, No. 4, 881-899
2024
Publisher: Learning Gate
DOI: 10.55214/25768484.v8i4.1468

Development of a photocell-based system supported by simulations for road vehicle counting and particle emissions estimation

João Garcia[1,2,3], Arian Semedo[1*]
[1]Instituto Superior de Engenharia de Lisboa R. Conselheiro Emídio Navarro, Lisbon, Portugal; ariansemedo1997@hotmail.com (A.S.).
[2]UnIRE, ISEL, Polytechnic University of Lisbon, Lisbon, Portugal.
[3]MARE-IPS, Marine and Environmental Sciences Centre, Escola Superior de Tecnologia, Instituto Politécnico de Setúbal, Setúbal, Portugal.

Abstract: This work presents the design and implementation of an innovative system that utilizes photocells for road vehicle counting and computational simulations to estimate traffic-related particulate (PM_{10}) emissions. The integration of photocell technology has resulted in a robust system with reduced counting errors, ensuring high accuracy in correlating traffic counts with emission values. The system was evaluated under various environmental conditions, demonstrating its effectiveness in providing reliable real-time data on the impact of road traffic on particle emissions. The methodology included the use of the ADMS-Urban model for emission estimation and simulations with Ansys Fluent, enabling the acquisition of dependable real-time data. The results indicate a strong agreement between measured and calculated PM_{10} concentrations, with the system maintaining precision comparable to direct observations. The observed values of 5.0 μg/m³ and 19.2% for absolute and relative errors, respectively, demonstrate the system's remarkable performance, supported by a robust correlation represented by R^2 = 0.88. This strong correlation underscores the reliability of the employed model, suggesting its capability to capture and explain a substantial portion of the variability in PM_{10} concentrations. Validation campaigns conducted on a street in Portugal confirmed the system's ability to accurately count vehicles and estimate particle emissions. The analysis revealed a significant agreement between measured and calculated average PM_{10} concentrations, with standard deviation values of 7.0 μg/m³ for measured concentrations and 7.5 μg/m³ for calculated concentrations, suggesting consistency between the datasets. These conclusions confirm that the system is a valuable tool for researchers and policymakers, providing crucial insights for the management and improvement of urban air quality, contributing to the development of urban planning policies and environmental sustainability.

1. Introduction

Air quality and its relationship with health are increasingly important aspects in understanding issues associated with everyday life[1], [2], [3]. These concerns become even more significant with demographic shifts and population aging, which necessitate new efforts in developing health, urban planning, and sustainable development policies at both local and global levels[4], [5]. These aspects are intricately linked, as good air quality is critical for human health and for maintaining the balance of the planet's environmental systems[5]. Conversely, it is well known that air pollution adversely affects the quality of life, impacting both social and public health [6], [7], [8]. One important aspect under debate is the adequate planning of cities, particularly concerning road traffic management[9]. Emissions of air pollutants from road traffic result from various processes, including combustion products from gasoline, diesel, and gas engines, as well as by products from vehicle oil, tire rubber, braking, bearings, car bodies, road materials, and the release of dust from the road and soil [10], [11].

* Correspondence: ariansemedo1997@hotmail.com

Traffic is a significant source of both fine particles and coarse particles, as well as condensable organic gases and nitrogen oxides, which subsequently form secondary nitrate aerosols [12], [13]. Particles of condensed carbonaceous material are primarily emitted by diesel vehicles but also by poorly functioning gasoline vehicles. Diesel engine emissions mainly consist of carbonaceous agglomerates smaller than 100 nm in diameter, while particles emitted by gasoline vehicles are typically smaller carbonaceous agglomerates, ranging from 10 nm to 80 nm [14] [15].

2. Particle Emissions Due to Traffic

Particle emissions from road traffic result from various processes, such as combustion products from gasoline, diesel, and gas engines; byproducts from vehicle oil; tire rubber; braking systems; bearings; car bodies; road materials; and the release of dust from the road and soil [16], [17]. Traffic is indeed a significant source of both fine (smaller) and coarse (larger) particles. Additionally, it emits condensable organic gases and nitrogen oxides, which subsequently form secondary nitrate aerosols[18]. Diesel vehicles primarily emit particles of condensed carbonaceous material, although poorly functioning gasoline vehicles also contribute. Diesel engine emissions mainly consist of carbonaceous agglomerates smaller than 100 nm in diameter, whereas gasoline vehicle emissions predominantly include smaller carbonaceous agglomerates ranging from 10 nm to 80 nm. While it is challenging to generalize conclusions about the association of various elements in atmospheric particles with their origin in road traffic, certain elements are frequently linked to such emissions. These elements include copper (Cu), zinc (Zn), lead (Pb), bromine (Br), iron (Fe), calcium (Ca), and barium (Ba) [19], [20], [21]. However, many metallic elements emitted from road traffic are not due to exhaust emissions (non-exhaust emissions) but originate from other vehicle sources such as tires, brakes, and other parts[22]. Additionally, the re-entry of previously deposited particles into the atmospheric air, known as resuspension, is a complex process initiated by mechanical disturbances such as wind, turbulence induced by road traffic, stress from passing tires, and construction activities[23].

The so-called "road dust" is an agglomeration of particles from various anthropogenic and biogenic sources [24]. On roads, this dust accumulates on the sides, near the sidewalk, and along central dividers. Resuspension, deposition, "washout" on and off the road, and the emission of new particles create a dynamic mechanism of "source" and "sink" of particle emission characterizing road traffic[25], [26]. Roads are among the largest sources of particle emissions in urban environments. Several studies have shown that resuspension is the predominant source of coarse particles in areas with heavy road traffic, significantly impacting particle concentrations in atmospheric air[27]. Although most resuspended particles are coarse, a small portion consists of fine particles [28]. The proportion of fine particles has two important implications with potentially significant consequences[29]. Firstly, fine particles can remain suspended much longer than coarse particles, resulting in a greater spatial impact on atmospheric particle concentrations. Secondly, the fine fraction of resuspended particles is more likely to contain constituents of anthropogenic origin, which may be more toxic than fine particles of natural origin.

3. Developed PM_{10} Traffic Emissions System

3.1. Architecture of system

To characterize road traffic and the corresponding particle emissions on urban roads, a road traffic counting method was developed using an automated system based on photocells, combined with traffic emission factors and Computational Fluid Dynamics (CFD) simulation.

Edelweiss Applied Science and Technology
ISSN: 2576-8484
Vol. 8, No. 4: 881-899, 2024
DOI: 10.55214/25768484.v8i4.1468

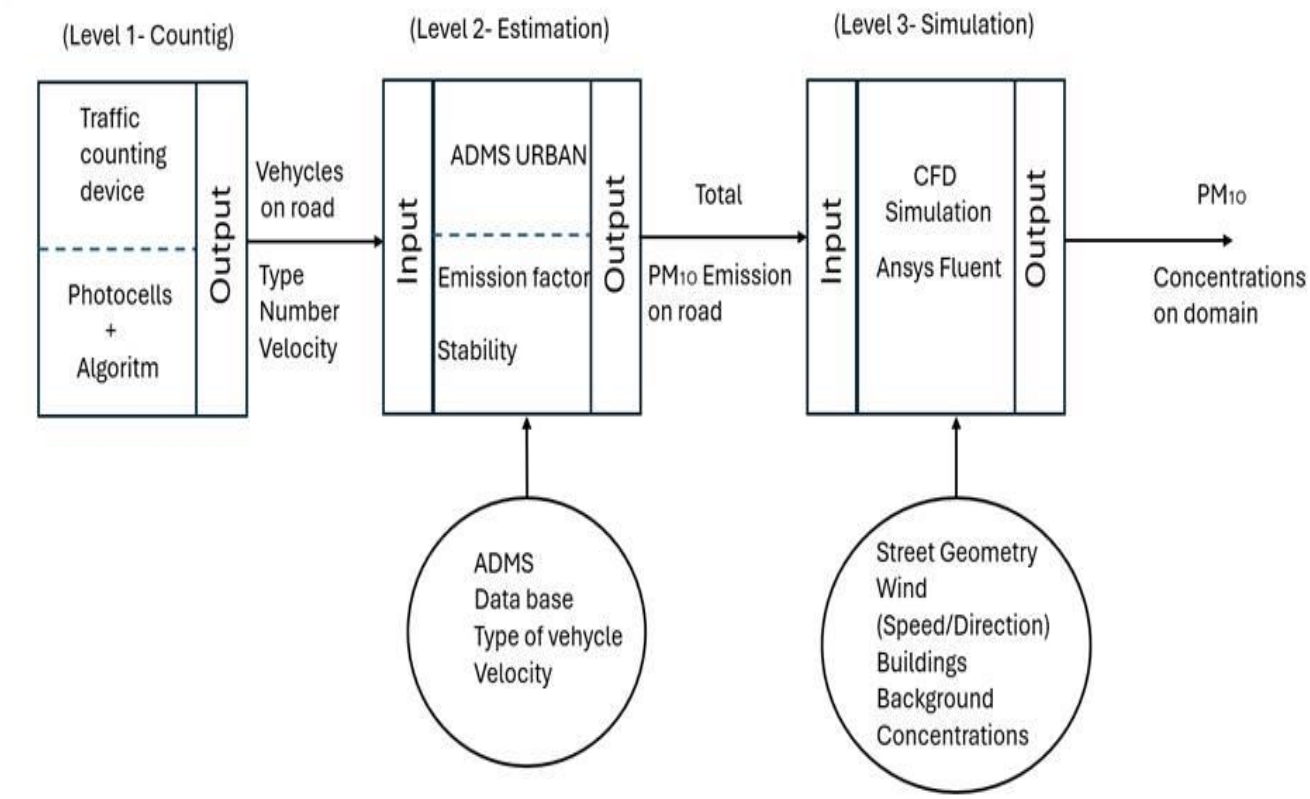

Figure 1.
General Architecture of the developed system.

Figure 1 illustrates the general architecture of the developed system, which comprises three levels. At level 1, the traffic counting device is identified. This device is responsible for counting vehicles on the road, identifying the number and type of vehicles, and measuring the speed of each vehicle. It consists of photocells supported by an algorithm. The output from this level includes the total number of each type of vehicle and their respective speeds during the counting period. A detailed description of this traffic counting device is provided in Section 3.2. At level 2, ADMS-Urban receives the information from the traffic counting device, including the number, type, and speed of the vehicles, as input parameters. Utilizing this information, ADMS-Urban applies its emission factors database to estimate the total PM10 emissions on the road (output). A detailed description of this level is provided in Section 3.3.

3.2. Road Traffic Counting System (Level 1)

To count the vehicles, a traffic counting device was developed as shown in Figure 2. This device comprises two long-range retro-reflective photocells manufactured by Omron, model E3G-L73 2M, a programmable logic controller (PLC) from Omron, model CP1L, and an HP laptop equipped with the necessary programming software. The primary objective of this system is to count vehicles circulating on the roadway, identify vehicle types (light or heavy), and measure their speed to accurately characterize PM10 emissions from traffic.

Edelweiss Applied Science and Technology
ISSN: 2576-8484
Vol. 8, No. 4: 881-899, 2024
DOI: 10.55214/25768484.v8i4.1468

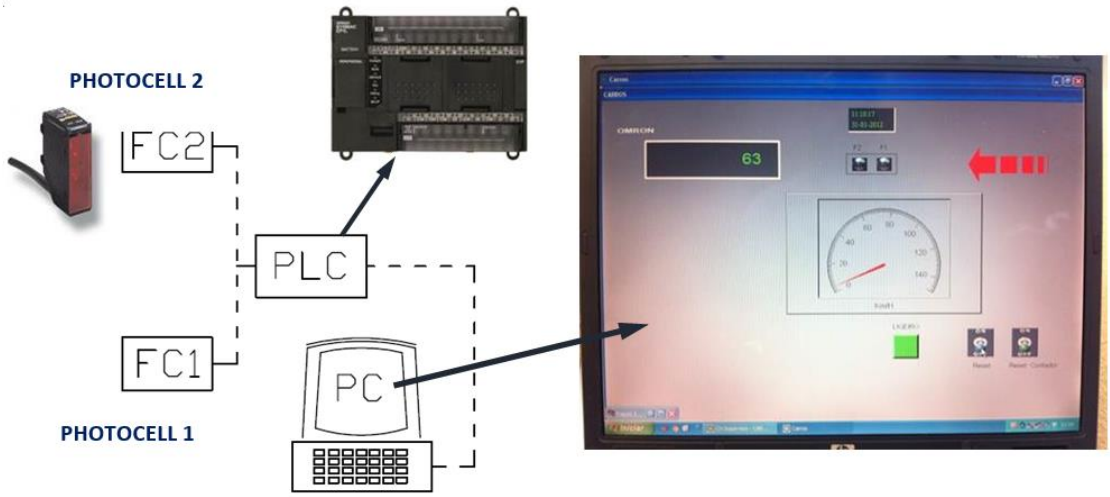

Figure 2.
Architecture of the developed road traffic counting device.

In Table 1, the main characteristics of the Omron E3G-L73 2M photocells are presented.

Table 1.
Key specifications of Omron E3G-L73 2M photocells.

Detection distance	0.2 m to 2 m (Adjustable)
Light source	Infrared LEDs
Electrical supply	10V to 13V
Operating temperature range	-25°C to 55°C
Degree of protection	IEC 60529; IP67
Response time	5 ms

In Table 2, the main characteristics of the Omron CP1L PLC photocells are presented.

Table 2.
Key specifications of Omron CP1L PLC (Omron, 2011).

Input points	12
Output points	8
Electrical supply	24 VDC
Operating temperature range	0°C to 55°C
Output type	Transistor
Execution speed	0.55 µs
Electrical power (consumption)	20W

This operational principle of the developed system for road traffic counting, focuses on the interaction of strategically positioned photocells alongside the road. During the operation of the photocells:

t1i – Time when the vehicle begins to pass through the 1st FC1 photocell(s)
t1f – Time when the vehicle finishes passing through the 1st FC1 photocell(s)
t2i – Time when the vehicle begins to pass through the 2nd FC2 photocell(s)
t2f – Time when the vehicle finishes passing through the 2nd FC2 photocell(s)
L - Distance between the two photocells (m)
vi - vehicle speed (m/s)

Edelweiss Applied Science and Technology
ISSN: 2576-8484
Vol. 8, No. 4: 881-899, 2024
DOI: 10.55214/25768484.v8i4.1468

ci – Length of each vehicle (m)

The system operates as follows:

Positioning of Photocells: Two photocells are installed alongside the road to detect vehicle passage through automatic beam reflection.

Operation of Photocell 1 (FC1): When a vehicle passes, the first photocell (FC1) is activated, initiating the time count (t1i). The count concludes when the vehicle completes passage, marking the time (t1f).

Operation of Photocell 2 (FC2): As the vehicle advances, it triggers the second photocell (FC2), initiating the time count (t2i). The count concludes when the vehicle completes passage through the second photocell, recording the time (t2f).

This method is essential for accurately calculating vehicle speed and length based on the times recorded by the photocells. This functionality is crucial for efficient traffic counting and precise monitoring, as depicted in Figure 3.

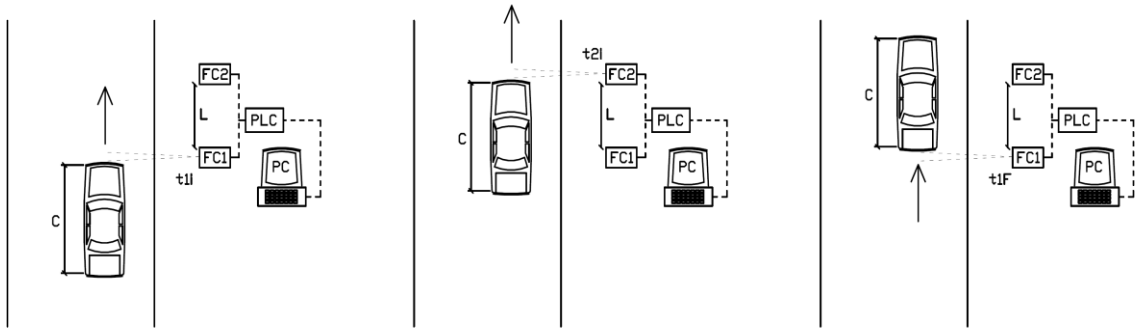

Figure 3.
Operating principle of the developed road traffic counting system.

This segment describes the process by which strategically positioned photocells alongside the road enable precise measurement of vehicle speed and length in real-time. Using the passage times recorded by the photocells, the system dynamically calculates the speed of each vehicle ($\boldsymbol{v_i}$) and, consequently, determines its length ($\boldsymbol{c_i}$). Additionally, the developed system automatically classifies vehicles based on their length, distinguishing between motorcycles, light vehicles, heavy goods vehicles, and heavy passenger vehicles, as defined by established criteria.

If we have the two photocells at a distance L, the speed of each vehicle is given by:

$$v_i = \frac{\Delta \mathrm{l}}{\Delta \mathrm{t}} = \frac{L}{t_{2i} - t_{1i}} \quad (1)$$

Knowing the speed v_i of each vehicle, of each vehicle, one can determine the c_i as:

$$c_i = v_i \Delta t_1 = v_i(t_{2i} - t_{2f}) \quad (2)$$

The photocells thus provide the variables t1i, t1f, t2i, t2f in real time to the computer. Subsequently, the developed program calculates and records in real-time the vehicle's identification number i, it is speed v_i , and it is the length c_i . The program further classifies each vehicle based on its type (light or heavy) determined by its length c_i, and records this information in a file.

To classify vehicles according to their length c_i, the following criteria were considered [30], [31], [32]:

- Motorcycles: 1.5 m < $c_i \leq$ 2.5 m
- Light: 2.5 m < $c_i \leq$ 5.5 m
- Heavy goods: 5.5 m < $c_i \leq$ 11 m
- Heavy passengers: 11 m < $c_i \leq$ 18 m

Edelweiss Applied Science and Technology
ISSN: 2576-8484
Vol. 8, No. 4: 881-899, 2024
DOI: 10.55214/25768484.v8i4.1468

3.3. PM_{10} Traffic Emissions Estimation (Level 2)

ADMS-Urban (Atmospheric Dispersion Modelling System) model was used to estimate particle emissions based on traffic counts obtained from the previously described system[33], [34]. Developed by Cambridge Environmental Research Consultants Ltd. (CERC), ADMS-Urban calculates pollutant concentrations from continuous emissions line sources (traffic). This advanced three-dimensional Gaussian model is integrated into a Lagrangian trajectory framework, accounting for the effects of major buildings, complex topography, atmospheric chemical reactions, plume rise over distance, long-range transport, and meteorological conditions. It has been extensively validated in numerous studies and is widely used by governments for strategic air quality decision-making. To utilize the ADMS-Urban model, particle emissions and their concentrations on the relevant roadways need to be estimated. The average emission values for each vehicle type are calculated. These values, along with average speed, vehicle type, and road type, are then entered as input data into the ADMS-Urban model, which computes the total particle emissions from road traffic on the specified road. The resulting PM_{10} emissions are then used as an input source in the Ansys Fluent CFD model (level 3). The model requires minimum data on road traffic, including the geographical locations of roads, traffic data, the size of buildings near traffic sources, the width of roads at traffic sources, meteorological data, wind direction and speed, and boundary layer parameters such as boundary layer height and Monin-Obukhov length. This data processing yields the average pollutant concentrations over a specific time interval. ADMS-Urban was specifically used to estimate emissions from road traffic, utilizing traffic data that include vehicle type, speed, the number of each type of vehicle, and pollutant emissions. Based on this data, the ADMS-Urban model uses the DMRB traffic emission factors database to calculate emissions from line sources, corresponding to road traffic. The input parameters for line sources (traffic) in ADMS-Urban are summarized in Table 3.

Table 3.
Input parameters in ADMS Urban for traffic sources.

Vehicle category	Type
Average speed	km/h
Vehicle count	Num/hr
Emission year	
Road elevation	m
Road width	m
Canyon eight	m

For line-type emissions originating from road traffic, the model considers the existence of buildings and accounts for additional turbulent flow within a street lined with buildings on both sides, following the Operational Street Pollution Model (OSPM) developed by the Danish Environmental Research Institute [35]. This model uses a simplified Gaussian plume approach to calculate pollutant concentrations within street canyons. Subsequently, the Ansys Fluent software is employed to calculate particle concentrations in the study domain.

3.4. Ansys Fluent Simulation (Level 3)

The software Ansys Fluent was utilized for Computational Fluid Dynamics (CFD) simulations to investigate the dispersion of PM_{10} in urban street (level 3). Ansys Fluent is a versatile commercial software widely used and continuously validated through comparisons with dispersion models [36] and wind tunnel experiments [37]. A spatial discretization of the computational domain was performed to achieve the study objectives, employing a tetrahedral grid particularly near buildings. The simulation involved a 3D flow analysis using a Lagrangian approach under steady-state conditions. Turbulence was modelled using the RNG k–epsilon model, which includes analytical formulations for turbulent

Edelweiss Applied Science and Technology
ISSN: 2576-8484
Vol. 8, No. 4: 881-899, 2024
DOI: 10.55214/25768484.v8i4.1468

Prandtl numbers and an analytically-derived differential formula for effective viscosity. A wind profile, turbulent kinetic energy, and turbulence dissipation rate were implemented as a user-defined function (UDF), considering a logarithmic law for the vertical wind profile. As described previously, regarding traffic emissions, the PM_{10} emission rates from vehicles on two-way streets were incorporated using outputs from the ADMS-Urban model (level 2), as described in Section 3.2. These emissions were introduced in Fluent as line sources, with the average number of vehicles during rush hours serving as the baseline scenario for traffic emissions. Background concentrations of other emissions within the domain were also considered.

4. PM_{10} Concentration Measurement Equipment

For the system validation and calibration, specific campaigns were conducted to measure particle concentrations in street, two distinct instruments were utilized: Verewa's Beta Dust F701-20 and the DustTrak model 8520. Verewa's Beta Dust F701-20 employs Beta radiation technology to continuously monitor and record particle concentrations in ambient air samples. The instrument features an automated system for collecting atmospheric air samples, where particles are captured on a paper filter for subsequent analysis. This method quantifies particle mass (mg) per cubic meter of humid air. During operation, the air sample is directed through a fiberglass tape cassette while the paper filter unwinds at a rate synchronized with the volumetric air flow measurement. Particles in the sample deposit onto the filter tape, which is then analysed radiometrically. The device utilizes a Beta emitter (C-14) and a Geiger-Müller counter for radiometric measurements. Particle mass is determined based on the attenuation of Beta radiation passing through the filter tape. Measurements are taken before and after the air sample passes through the filter, providing intensity readings that correlate with the particle layer thickness on the filter surface assuming uniform distribution. To calculate particle concentration, the mass of particles collected is divided by the sampled air volume. The procedure begins with calibrating the system to a clean filter section for an initial zero reading. The filter section is then exposed to ambient air, closed, and sampled using a disc vacuum pump with a nominal flow rate of 1 m3/h to capture particles. Subsequently, the filter section is repositioned for a second measurement where particle concentration is determined based on the difference in Beta radiation intensity between the clean and particle-laden filter sections. This intensity difference is detected by the Geiger-Müller counter and processed by a microprocessor, displaying particle concentration in micrograms per cubic meter (µg/m3). The operational diagram of Verewa's Beta Dust F701-20 particle concentration measuring equipment is illustrated in Figure 4.

Edelweiss Applied Science and Technology
ISSN: 2576-8484
Vol. 8, No. 4: 881-899, 2024
DOI: 10.55214/25768484.v8i4.1468

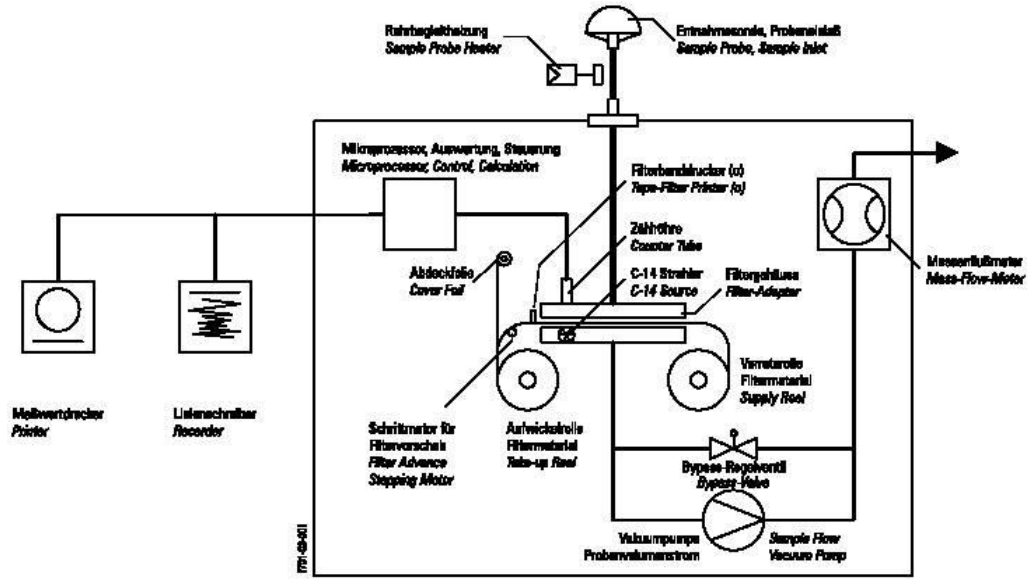

Figure 4.
Operating diagram of Verewa's Beta Dust F701-20 particle concentration measuring equipment.

Figure 5 shows the particle collection filter used for collecting air samples in the particle concentration measuring equipment, Verewa's Beta Dust F701-20.

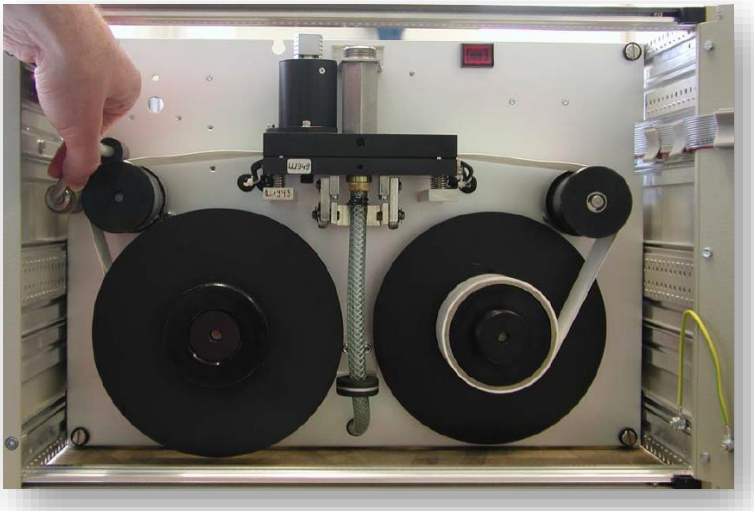

Figure 5.
Filter for collecting samples of particles in the air, from the particle concentration measuring equipment Verewa's Beta Dust F701-20.

The Verewa's Beta Dust F701-20 equipment is capable of measuring particles with diameters less than 10 μm (PM_{10}), 2.5 μm ($PM_{2.5}$), and total suspended particles (TSP), using the sampling head located in the collection tube, which is appropriately calibrated for the intended purpose (Figure 6). As

Edelweiss Applied Science and Technology
ISSN: 2576-8484
Vol. 8, No. 4: 881-899, 2024
DOI: 10.55214/25768484.v8i4.1468

for monitoring periods, these can be adjusted according to user needs, ranging from 30 minutes to 24 hours.

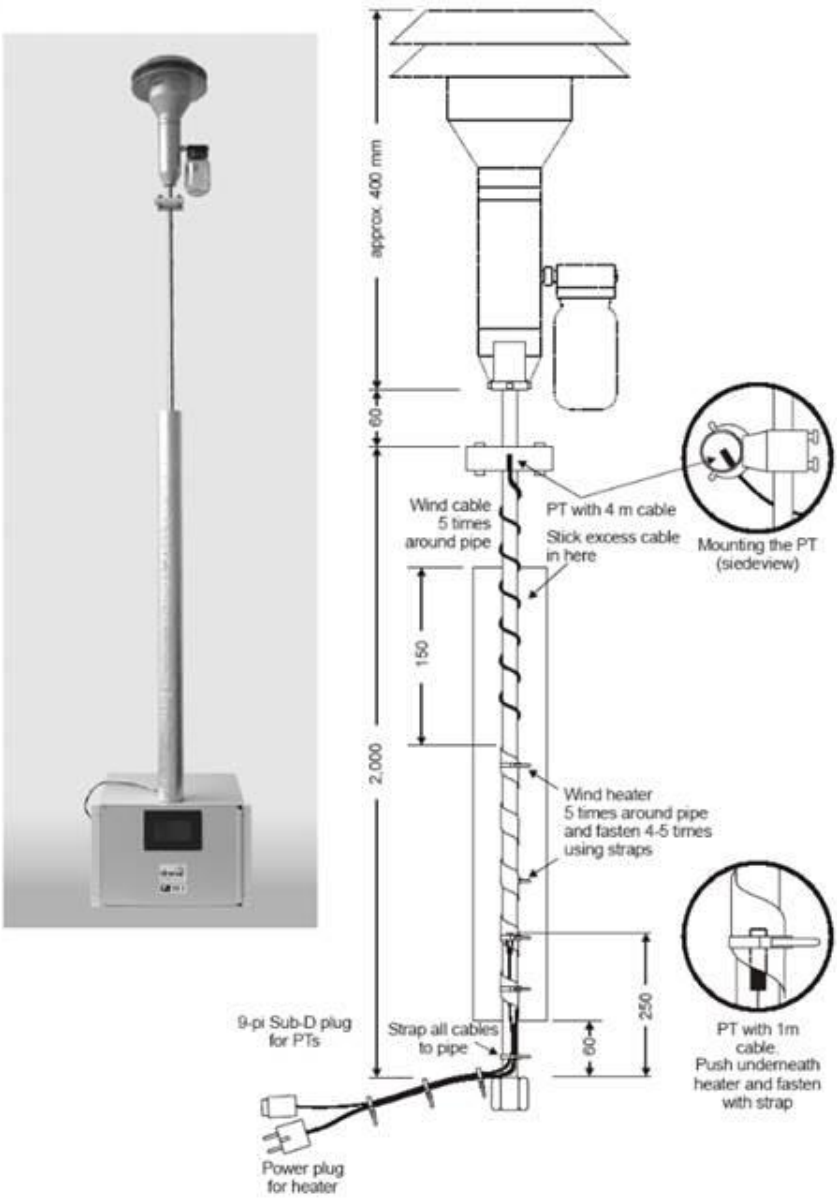

Figure 6.
Collection tube and sampling head of Verewa's Beta Dust F701-20 particle concentration measuring equipment.

Table 4 presents the main technical characteristics of the Verewa's Beta Dust F701-20 equipment.

Edelweiss Applied Science and Technology
ISSN: 2576-8484
Vol. 8, No. 4: 881-899, 2024
DOI: 10.55214/25768484.v8i4.1468

Table 4.
Key technical specifications of the Verewa's Beta Dust F701-20 particle concentration measuring equipment adapted from.

Range	$PM_{2,5}$ – PM_{10} - TSP
Lower detection threshold	0.001 mg/m^3
Precision	± 2%
Electrical supply	230 V/50 Hz ±10%; 110V/60Hz ± 10%
Required electrical power	0.4 kVa
Operating temperature range	0 ºC – 50 ºC
Signal output	4 – 20 mA, 3x RS-232, Gesytec protocol
Detector	Geiger-Muller-counter-tube
Filter (Material)	Fibreglass-filter 99.95%
Sampling flow	1000 l/h
Sampling flow rate accuracy	±5%
Sampling system	VDI 2463, EN12341
Pump type	Disco
Pump flow rate (Nominal)	1 m^3/h
Dimensions	320mm x 450mm x 500mm
Weight	26kg

Another device used in particle concentration measurement campaigns was the DustTrak model 8520 equipment, manufactured by TSI (Figure 7). This equipment performs real-time measurement of particle concentration in ambient air using the laser photometry sensor method. It is capable of measuring particle concentrations corresponding to PM_{10}, $PM_{2.5}$, $PM_{1.0}$.

Figure 7.
Dust track 8520 particle concentration measuring equipment (TSI, 2006).

Edelweiss Applied Science and Technology
ISSN: 2576-8484
Vol. 8, No. 4: 881-899, 2024
DOI: 10.55214/25768484.v8i4.1468

Real-time measurements are performed using laser photometry, a method that involves counting mass using a laser lamp. A small suction pump drives the sample flow through an optical chamber, where the sample is exposed to a focused laser beam. Particles within the optical chamber scatter light in all directions, and a 90º lens collects the scattered light and directs it onto a photodetector for concentration measurement. The detection circuit converts light into a potential difference proportional to the sample's mass concentration. This potential difference is processed by the equipment's processor and scaled by an internal calibration constant to determine the mass concentration in μg/m³. Figure 8 illustrates the simplified operational diagram of the DustTrak 8520 equipment.

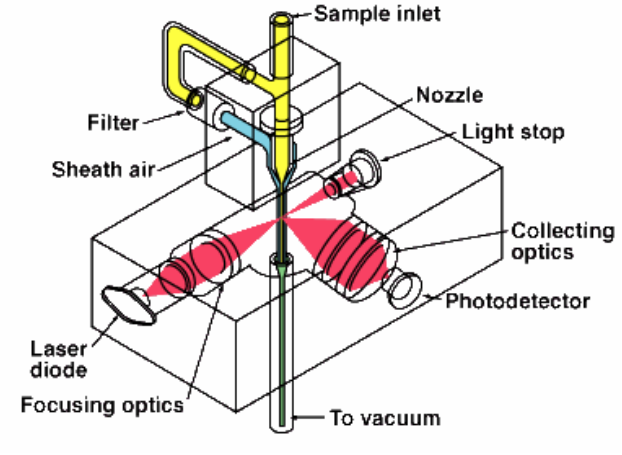

Figure 8.
Operating diagram of the Dust track 8520 equipment.

Table 5 presents the main characteristics of the DustTrak 8520 particle concentration measuring equipment.

Table 5.
Key technical specifications of the DustTrak 8520 (TSI, 2006).

Range	0.001 to 100 mg/m³
Resolution	± 0.1% reading or ± 0.001 mg/m³
Operating temperature range	0°C – 50°C
Detector	90º light scattering
Sampling flow	Adjustable 1.4 to 2.4 l/min (1.7 l/min nominal)
Range of application (particle diameter)	0.1 to 10 μm

5. Data Collection

5.1. Traffic Counting System

A traffic data collection campaign was conducted on Avenida do Bocage (38°39'20.93"N; 9°03'45.63"W) in the city of Barreiro, Lisbon. This road experiences heavy traffic in both directions and is lined with residential buildings, offices, and services, serving as a primary access route to the city. The data collection occurred during peak and off-peak hours. During these campaigns, the following variables were recorded: vehicle counts, vehicle types (such as light vehicles, heavy goods vehicles, heavy passenger vehicles, and motorcycles), fuel types used, road characteristics (urban or expressway), road width, building heights adjacent to the road, and average vehicle speeds. Figure 9 depicts the operational traffic counting system developed on Avenida do Bocage.

Edelweiss Applied Science and Technology
ISSN: 2576-8484
Vol. 8, No. 4: 881-899, 2024
DOI: 10.55214/25768484.v8i4.1468

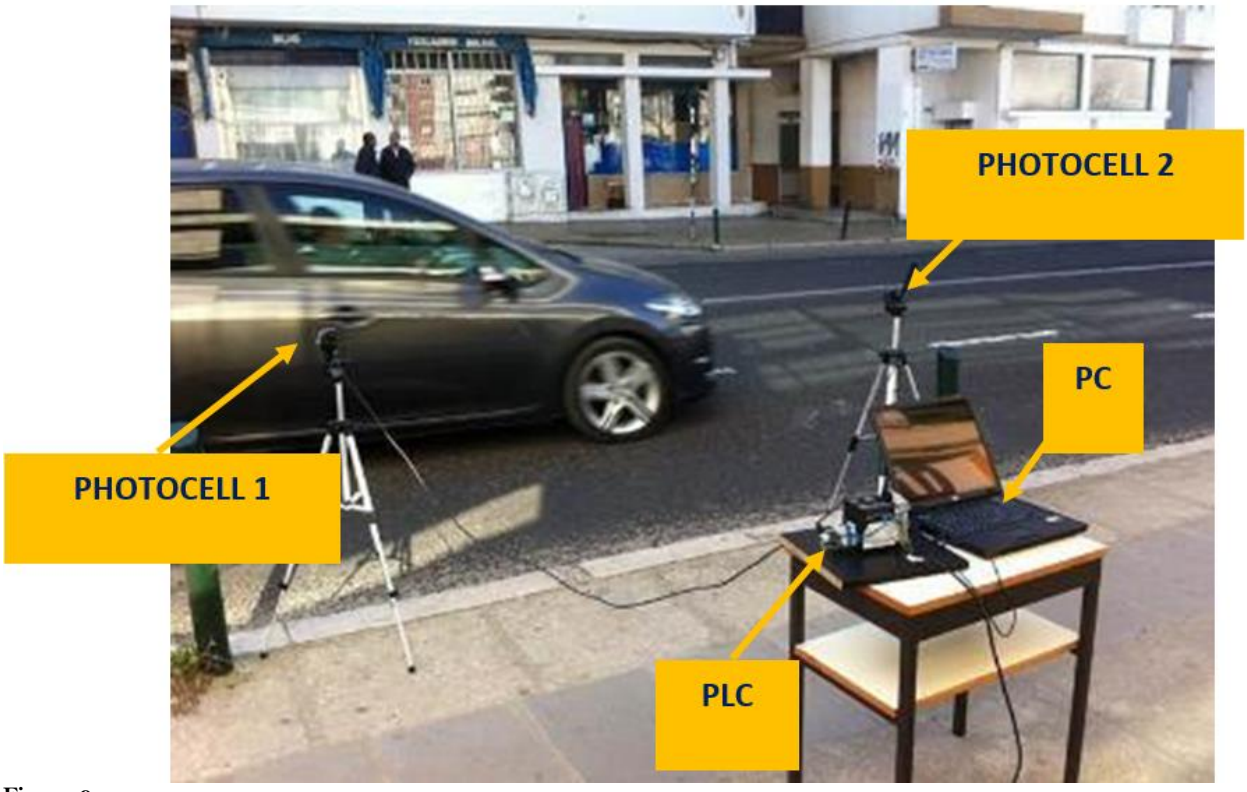

Figure 9.
Traffic counting system in operation on Avenida do bocage.

Table 6 presents the results of the counts conducted using the developed system on Avenida do Bocage for the two distinct periods.

Table 6.
Characterisation of vehicle counts carried out on Av. do Bocage.

	Type and number of vehicles/h				Total vehicles (per hour)
Score	**Light**	**Heavy loads**	**Heavy passenger trucks**	**Motorcycles**	
Period 1	3050	78	94	22	3244
Period 2	2933	69	43	29	3074

The counts presented in Table 6 demonstrate a considerable amount of road traffic during the analysed periods, highlighting the diversity and volume of vehicles circulating in the studied area.

6. Fluent Simulation

Following the completion of traffic counting and monitoring campaigns, aimed at estimating PM_{10} concentrations resulting from road traffic emissions, a Fluent simulation was executed. The simulation utilized a calculation domain centered on Av. do Bocage, with dimensions of 715 m x 300 m x 150 m (Figure 10). The simulation integrated average vehicle counts and types determined by the developed counting system.

Edelweiss Applied Science and Technology
ISSN: 2576-8484
Vol. 8, No. 4: 881-899, 2024
DOI: 10.55214/25768484.v8i4.1468

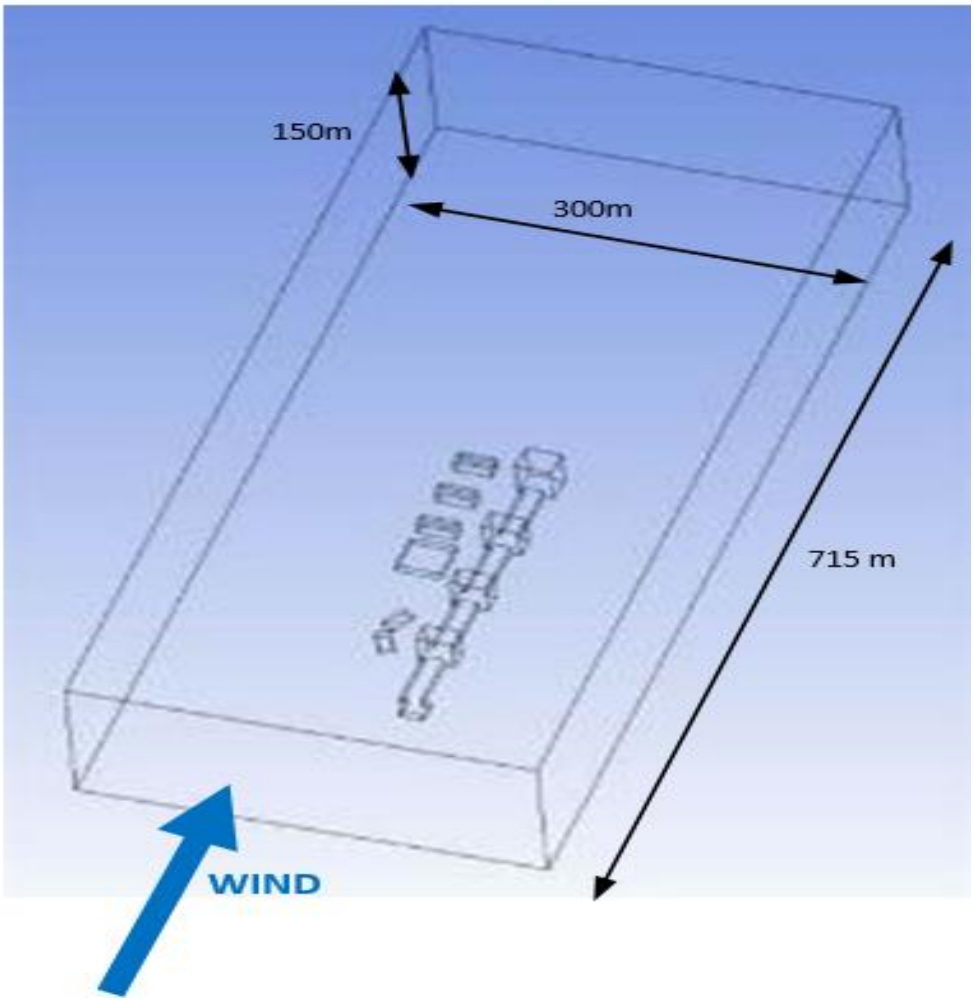

Figure 10.
Representation of the domain under study for cases of west wind.

The implemented mesh type was an unstructured hybrid mesh of Tetrahedral type, consisting of tetrahedral, hexahedral, pyramidal, and wedge cells. This mesh type is widely employed in scenarios with complex geometries due to its optimal balance between accuracy and computational efficiency. Given the anticipated stronger wind speed gradients near buildings, the mesh was specifically refined in these areas. Initially, the mesh element size near building walls was set to 1 meter, with a growth rate of 1.2 indicating subsequent layer mesh element increments. This resulted in a 20% size increase per layer, culminating in a maximum element size of 6 meters at the mesh edge cell. Additionally, the ground-adjacent region underwent height refinement, with the first layer starting at 0.8 meters above ground level and subsequent layers extending up to 6 meters, except in refined sections. This approach resulted in a mesh whose characteristics are summarized in Table 7 and depicted in figure 11, illustrating the mesh developed in Ansys Fluent software.

Edelweiss Applied Science and Technology
ISSN: 2576-8484
Vol. 8, No. 4: 881-899, 2024
DOI: 10.55214/25768484.v8i4.1468

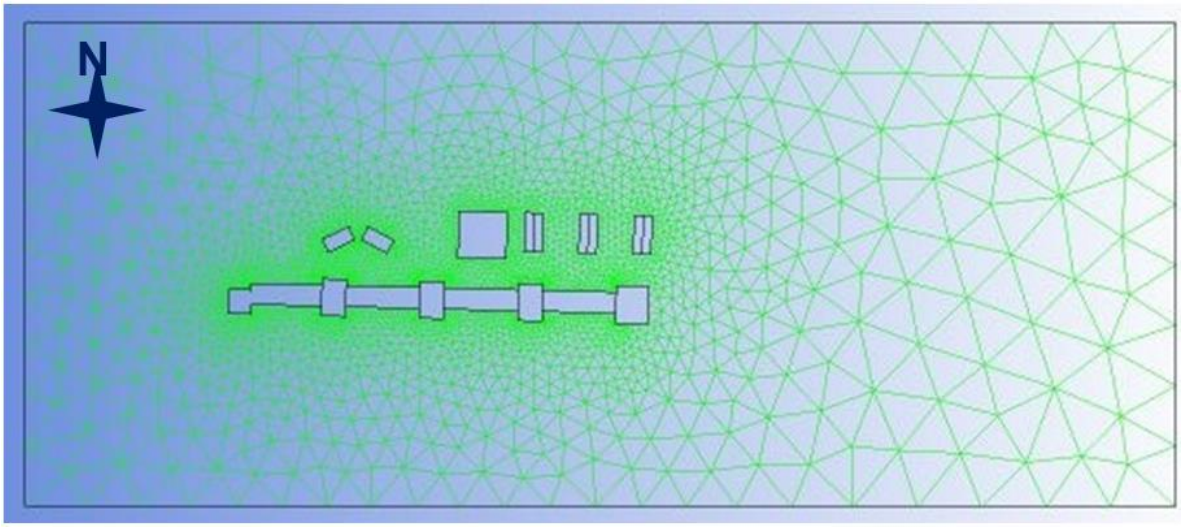

Figure 11.
Mesh representation.

Table 7.
Characterisation of the number of nodes and cells for the current configuration and for the 4 wind directions considered.

Scenario	No. of cells				No. of knots			
	E	W	N	S	E	W	N	S
Street configuration	202531	201354	202672	201195	37658	37303	37543	37260

Boundary conditions were selected to accurately model airflow dynamics considering the prevailing wind direction. A no-slip condition was applied to all solid surfaces, including the ground and building walls, ensuring realistic interaction between air and surfaces. Symmetry conditions were implemented on the upper and lateral boundaries of the domain, assuming zero flow for all variables along these planes. At the domain entrances, aligned with wind direction, a logarithmic wind speed profile was applied to represent the atmospheric boundary layer's evolution with height. This profile followed a logarithmic law typical for urban environments, with a power law exponent (Von Karman constant) set to 0.42. For the domain exit section, a free boundary condition allowed airflow and pressure to exit without constraint, reflecting real-world conditions. These boundary conditions (Figure 12) are standard in studies focusing on pollutant dispersion within urban street canyons.

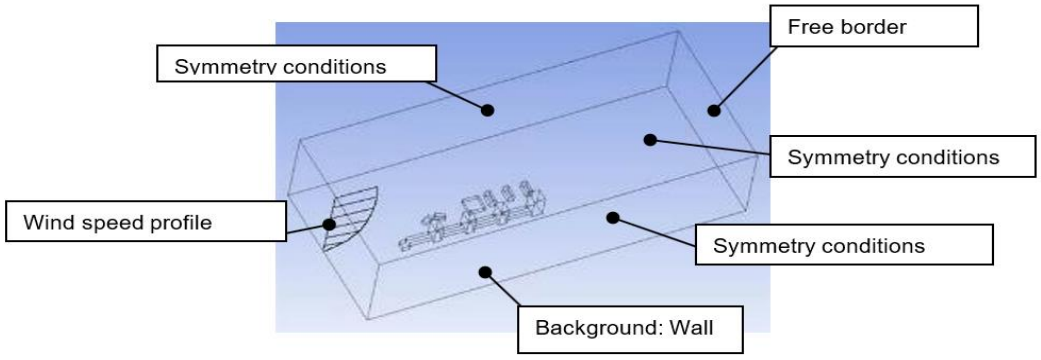

Figure 12.
Boundary conditions considered.

Edelweiss Applied Science and Technology
ISSN: 2576-8484
Vol. 8, No. 4: 881-899, 2024
DOI: 10.55214/25768484.v8i4.1468

PM_{10} emissions from road traffic were incorporated into the Ansys Fluent model as two area-type sources positioned at a height of 0.1 m, corresponding to the median plane of vehicle exhaust emissions. Each source represented one direction of the road on Avenida do Bocage. The PM_{10} emission rate introduced into these area sources, derived from results obtained from the ADMS-Urban model, was 1.82 x 10^-6 kg/s for each road direction. Table 8 provides an overview of the emission values used in the Ansys Fluent study.

Table 8.
Summary of the emission rate considered for the two area sources.

Emission factor ADMS-urban (g/km/s)	Road length (km)	Emission total (kg/s)	Issuance for each route (kg/s)
1.35 x 10-2	0.27	3.65 x 10-6	1.82 x 10-6

Particle emissions were introduced into these two area sources at a constant emission rate, modelled as inert, uniform material with properties similar to anthracite (density mass of 1500 kg/m³). Recent research on the chemical composition of road traffic emissions indicates that approximately 97% of particles emitted from diesel vehicles are carbonaceous, while in gasoline vehicles, this percentage decreases to 89% [38], [39], [40]. Studies characterizing the size distribution of particles resulting from vehicle emissions suggest a log-normal distribution with a peak near 0.5 µm [41]. No chemical reactions were considered for these particles due to their inert nature, and transformation processes were disregarded, as they are typically negligible at the scale of street canyons.

7. Results and System Validation

7.1. Measured PM_{10} Concentrations

To validate the developed system, PM_{10} concentration measurements were conducted at seven monitoring points as depicted in Figure 13. These points are distributed as follows: Point 1 is situated near the school network area. Point 2 is located adjacent to the Barreirense Bingo establishment. Point 3 is positioned in the middle of the residential parking blocks. Point 4 is situated at the end of the residential parking blocks. Point 5 is marked at the corner adjacent to a tall pink building. Point 6 is positioned at the corner of residential buildings on the east side. Point 7 is located at the corner of residential buildings on the west side. Figure 13 illustrates the street under study, highlighting its main buildings, along with the locations of the monitoring and measurement points.

Figure 13.
PM_{10} concentration (Monitoring points).

Edelweiss Applied Science and Technology
ISSN: 2576-8484
Vol. 8, No. 4: 881-899, 2024
DOI: 10.55214/25768484.v8i4.1468

Table 9 shows the PM_{10} concentration values measured in the campaign at the control point 1 for a sampling period with a 10-minute interval.

Table 9.
PM_{10} measured concentrations.

Hour	8h00	8h10	8h20	8h30	8h40	8h50	9h00	9h10	9h20	9h30	9h40	9h50	10h	10h10	10h20	10h30	10h40	10h50	11h
Measured concentrations (µg/m3)	23	27	29	26	28	23	25	29	25	26	24	25	24	25	23	21	22	19	18
Hour	11h10	11h20	11h30	11h40	11h50	12h	12h10	12h20	12h30	12h40	12h50	13h	13h10	13h20	13h30	13h40	13h50	14h	14h10
Measured concentrations (µg/m3)	17	18	16	15	13	12	14	16	21	19	22	24	25	23	22	19	18	19	17
Hour	14h20	14h30	14h40	14h50	15h	15h10	15h20	15h30	15h40	15h50	16h	16h10	16h20	16h30	16h40	16h50	17h	17h10	17h20
Measured concentrations (µg/m3)	15	12	11	13	12	11	13	14	15	14	15	16	14	17	19	22	21	23	24
Hour	17h30	17h40	17h50	18h	18h10	18h20	18h30	18h40	18h50	19h	19h10	19h20	19h30	19h40	19h50	20h	20h10	20h20	20h30
Measured concentrations (µg/m3)	26	27	29	31	33	35	34	35	31	27	25	26	24	21	19	18	17	19	15
Hour	20h40	20h50	21h	21h10	21h20	21h30	21h40	21h50	22h	22h10	22h20	22h30	22h40	22h50	23h	23h10	23h20	23h30	23h40
Measured concentrations (µg/m3)	15	16	14	14	13	12	11	10	11	12	9	8	9	8	8	9	7	8	9

7.2. Results

In this subsection, a plot graph depicting measured and calculated PM_{10} concentrations is presented (Figure 14). The comparative results between the two methods for determining PM_{10} concentrations display average values measured on Avenida do Bocage and those calculated by the model for Control Point 1 (school area) at a height of 1.5 m.

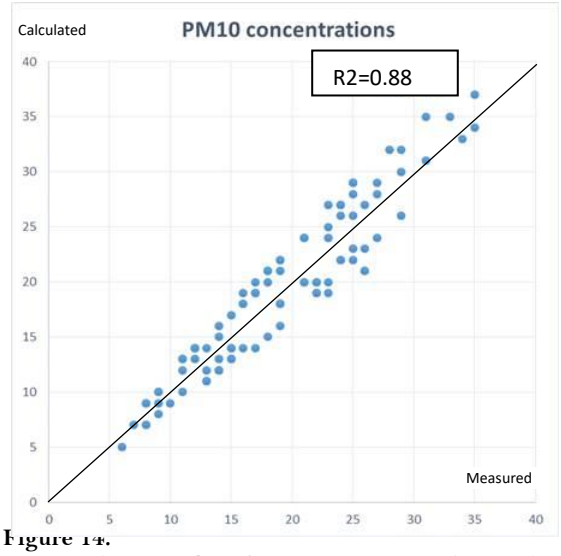

Figure 14.
Comparative graph of PM_{10} concentration values measured and calculated

Edelweiss Applied Science and Technology
ISSN: 2576-8484
Vol. 8, No. 4: 881-899, 2024
DOI: 10.55214/25768484.v8i4.1468

Analysis of Figure 14 confirms a strong agreement between the average PM_{10} concentrations measured on Avenida do Bocage and those calculated by the developed system. To assess the accuracy of these results, a linear relationship between observed and predicted values was determined. The coefficient of determination (R^2), which measures the model's fit to the observed data, was found to be 0.88. This indicates that 88% of the variability in the observed data can be explained by the developed model, demonstrating high precision and predictive capability. Figure 14 illustrates a comparative graph of PM_{10} concentration values measured at all control points (Points 1 to 7) during the two validation campaigns. The strong correlation observed reinforces the reliability of the developed system in predicting PM_{10} concentrations on the road. This robust agreement suggests that the model effectively captures a significant portion of the variability in PM_{10} concentrations, enhancing the validity and practical applicability of the results. Table 10 summarizes descriptive statistical values from the comparison between measured and calculated concentrations by the developed system.

Table 10.
Summary of statistical parameters (Measured versus calculated PM_{10} concentrations).

Average measured concentrations ($\mu g/m^3$)	Average calculated concentrations ($\mu g/m^3$)	Standard deviation of measured concentrations ($\mu g/m^3$)	Standard deviation calculated concentrations ($\mu g/m^3$)	Maximum absolute error ($\mu g/m^3$)	Maximum relative error
18.9	19.1	7.0	7.4	5.0	19.2%

Upon reviewing the values presented in Table 10, it is evident that the standard deviations of 7.0 $\mu g/m^3$ for the measured concentrations and 7.5 $\mu g/m^3$ for the calculated concentrations indicate a relative consistency between the two datasets. This consistency suggests that the developed system maintains accuracy comparable to direct observation. Furthermore, the recorded values of 5.0 $\mu g/m^3$ and 19.2% for absolute and relative errors, respectively, signify good performance of the developed system. These metrics demonstrate the system's ability to effectively estimate PM_{10} concentrations with a low margin of error, reinforcing its reliability and suitability for practical applications.

8. Conclusions

An innovative system for vehicle counting on roads and estimating particulate matter (PM_{10}) emissions using photocells and computational simulations has been presented. The system proved highly effective in accurately counting vehicles and estimating particulate emissions under various environmental conditions. The integration of photocells and the application of the ADMS-Urban model for emission estimation, followed by simulations with Ansys Fluent, enabled the acquisition of reliable real-time data. The validation campaigns conducted in a street of Portugal, demonstrated that the developed system is capable of accurately counting vehicles and estimating particulate emissions. Analysis of the results showed significant agreement between the measured and calculated average PM_{10} concentrations. The absolute and relative errors of 5.0 $\mu g/m^3$ and 19.2%, respectively, highlight the system's good performance. The comparison between measured and calculated PM_{10} concentrations revealed a strong correlation, represented by a determination coefficient (R^2) of 0.88. This robust correlation underscores the reliability of the employed model, indicating its ability to capture and explain a substantial portion of the variability in PM_{10} concentrations. These results are essential for the validation and practical applicability of the system. The standard deviation values of 7.0 $\mu g/m^3$ for measured concentrations and 7.5 $\mu g/m^3$ for calculated concentrations suggest a relative consistency between the two data sets. This consistency reinforces the system's accuracy, demonstrating its ability to provide estimates comparable to direct observations. The findings of this study confirm that the developed system is a valuable tool for researchers and policymakers, offering crucial insights for urban air quality management and improvement. The strong correlation and observed consistency indicate

Edelweiss Applied Science and Technology
ISSN: 2576-8484
Vol. 8, No. 4: 881-899, 2024
DOI: 10.55214/25768484.v8i4.1468

that the system can be effectively used to assess the impact of road traffic on particulate emissions, contributing to the development of urban planning policies and environmental sustainability.

References
[1] H. I. Abdel-Shafy and M. S. M. Mansour, "A review on polycyclic aromatic hydrocarbons: Source, environmental impact, effect on human health and remediation," *Egyptian Journal of Petroleum*, vol. 25, no. 1, pp. 107–123, Mar. 2016, doi: 10.1016/j.ejpe.2015.03.011.

[2] R. Aguilera, T. Corringham, A. Gershunov, and T. Benmarhnia, "Wildfire smoke impacts respiratory health more than fine particles from other sources: observational evidence from Southern California," *Nat Commun*, vol. 12, no. 1, Dec. 2021, doi: 10.1038/s41467-021-21708-0.

[3] Y. Guo *et al.*, "The burden of lung cancer mortality attributable to fine particles in China," *Science of The Total Environment*, vol. 579, pp. 1460–1466, Feb. 2017, doi: 10.1016/j.scitotenv.2016.11.147.

[4] American Lung Association, "State of the Air 2021," 2021, 2021. Accessed: Jul. 21, 2024. [Online]. Available: https://www.lung.org/getmedia/17c6cb6c-8a38-42a7-a3b0-6744011da370/sota-2021.pdf

[5] S. C. Anenberg *et al.*, "Global air quality and health co-benefits of mitigating near-term climate change through methane and black carbon emission controls," *Environ Health Perspect*, vol. 120, no. 6, pp. 831–839, Jun. 2012, doi: 10.1289/ehp.1104301.

[6] M. Kuntic, I. Kuntic, O. Hahad, J. Lelieveld, T. Münzel, and A. Daiber, "Impact of air pollution on cardiovascular aging," *Mech Ageing Dev*, vol. 214, Sep. 2023, doi: 10.1016/j.mad.2023.111857.

[7] E. W. Butt *et al.*, "Global and regional trends in particulate air pollution and attributable health burden over the past 50 years," *Environmental Research Letters*, vol. 12, no. 10, Oct. 2017, doi: 10.1088/1748-9326/aa87be.

[8] H. Carvalho, "New WHO global air quality guidelines: more pressure on nations to reduce air pollution levels," *Lancet Planet Health*, vol. 5, no. 11, pp. e760–e761, Nov. 2021, doi: 10.1016/S2542-5196(21)00287-4.

[9] C. S. Malley, E. N. Lefèvre, J. C. I. Kuylenstierna, S. Haeussling, I. C. Howard, and N. Borgford-Parnell, "Integration of Short-Lived Climate Pollutant and air pollutant mitigation in nationally determined contributions," *Climate Policy*, vol. 23, no. 10, pp. 1216–1228, Nov. 2023, doi: 10.1080/14693062.2022.2125928.

[10] I. Vouitsis *et al.*, "Transport-related airborne nanoparticles: Sources, different aerosol modes, and their toxicity," *Atmos Environ*, vol. 301, May 2023, doi: 10.1016/j.atmosenv.2023.119698.

[11] M. Crippa *et al.*, "GHG EMISSIONS OF ALL WORLD COUNTRIES JRC SCIENCE FOR POLICY REPORT," doi: 10.2760/235266.

[12] L. Qi *et al.*, "Source identification and characterization of organic nitrogen in atmospheric aerosols at a suburban site in China," *Science of the Total Environment*, vol. 818, Apr. 2022, doi: 10.1016/j.scitotenv.2021.151800.

[13] Y. Fujitani *et al.*, "Contribution of industrial and traffic emissions to ultrafine, fine, coarse particles in the vicinity of industrial areas in Japan," *Environmental Advances*, vol. 5, Oct. 2021, doi: 10.1016/j.envadv.2021.100101.

[14] A. M. Ansari, L. A. Memon, and M. Y. E. Selim, "Experimental study of particulate matter emission for a diesel engine fueled with nanoparticles and biofuel / diesel blends," *International Journal of Thermofluids*, vol. 23, Aug. 2024, doi: 10.1016/j.ijft.2024.100738.

[15] P. Karjalainen *et al.*, "Exhaust particles of modern gasoline vehicles: A laboratory and an on-road study," *Atmos Environ*, vol. 97, pp. 262–270, 2014, doi: 10.1016/j.atmosenv.2014.08.025.

[16] D. C. S. Beddows, R. M. Harrison, T. Gonet, B. A. Maher, and N. Odling, "Measurement of road traffic brake and tyre dust emissions using both particle composition and size distribution data," *Environmental Pollution*, vol. 331, Aug. 2023, doi: 10.1016/j.envpol.2023.121830.

[17] M. Tahiri and M. Inchaouh, "Air pollution due to road transportation in Morocco: evolution and impacts," *Journal of Multidisciplinary Engineering Science and Technology (JMEST)*, vol. 4, pp. 2458–9403, 2017, [Online]. Available: www.jmest.org

[18] I. M. Errigo *et al.*, "Human Health and Economic Costs of Air Pollution in Utah: An Expert Assessment," *Atmosphere (Basel)*, vol. 11, no. 11, p. 1238, Nov. 2020, doi: 10.3390/atmos11111238.

[19] R. M. Hoesly *et al.*, "Historical (1750–2014) anthropogenic emissions of reactive gases and aerosols from the Community Emissions Data System (CEDS)," *Geosci Model Dev*, vol. 11, no. 1, pp. 369–408, Jan. 2018, doi: 10.5194/gmd-11-369-2018.

[20] M. Ogrizek, A. Kroflič, and M. Šala, "Critical review on the development of analytical techniques for the elemental analysis of airborne particulate matter," *Trends in Environmental Analytical Chemistry*, vol. 33, p. e00155, Mar. 2022, doi: 10.1016/j.teac. 2022.e00155.

[21] J. Zhang, L. Wu, Y. Zhang, F. Li, X. Fang, and H. Mao, "Elemental composition and risk assessment of heavy metals in the PM10 fractions of road dust and roadside soil," *Particuology*, vol. 44, pp. 146–152, Jun. 2019, doi: 10.1016/j.partic.2018.09.003.

[22] N. C. Nkosi, R. P. Burger, C. Pauw, N. Ayob, and S. J. Piketh, "The impact of vehicle parameters on road PM10 vehicle resuspended emissions: A case in South African low-income settlement," *Clean Air Journal*, vol. 33, no. 2, Dec. 2023, doi: 10.17159/caj/2023/33/2.15497.

[23] G. Valotto, D. Zannoni, P. Guerriero, G. Rampazzo, and F. Visin, "Characterization of road dust and resuspended particles close to a busy road of Venice mainland (Italy)," *International Journal of Environmental Science and Technology*, vol. 16, no. 11, pp. 6513–6526, Nov. 2019, doi: 10.1007/s13762-019-02246-1.

[24] D. J. Bryant *et al.*, "Biogenic and anthropogenic sources of isoprene and monoterpenes and their secondary organic 1 aerosol in Delhi, India 2", doi: 10.5194/acp-2022-603.

[25] J.-H. TSAI and Y.-L. WU, "CONTRIBUTIONS OF ROAD DUST RESUSPENSION TO THE AIRBORNE PARTICLE CONCENTRATIONS IN TAIPEI," *Particulate Science and Technology*, vol. 13, no. 1, pp. 55–67, Jan. 1995, doi: 10.1080/02726359508906670.

[26] N. Dang, H. Zhang, H. Li, M. M. A. Salam, and G. Chen, "Comprehensive Evaluation of Dust Retention and Metal Accumulation by the Leaves of Roadside Plants in Hangzhou among Seasons," *Forests*, vol. 13, no. 8, p. 1290, Aug. 2022, doi: 10.3390/f13081290.

[27] A. J. Thorpe, R. M. Harrison, P. G. Boulter, and I. S. McCrae, "Estimation of particle resuspension source strength on a major London Road," *Atmos Environ*, vol. 41, no. 37, pp. 8007–8020, Dec. 2007, doi: 10.1016/j.atmosenv.2007.07.006.

[28] F. Wagenpfeil, H. G. Paretzke, J. M. Peres, and J. Tschiersch, "Resuspension of coarse particles in the region of Chernobyl," *Atmos Environ*, vol. 33, no. 20, pp. 3313–3323, Sep. 1999, doi: 10.1016/S1352-2310(98)00293-3.

[29] T. Skuland *et al.*, "Road tunnel-derived coarse, fine and ultrafine particulate matter: physical and chemical characterization and pro-inflammatory responses in human bronchial epithelial cells," *Part Fibre Toxicol*, vol. 19, no. 1, p. 45, Dec. 2022, doi: 10.1186/s12989-022-00488-5.

[30] J. Garcia, R. Cerdeira, L. Coelho, and N. Tavares, "Studying Street geometry influence in PM10 concentration," *Int. J. Environment and Pollution*, vol. 50, pp. 283–292, 2012, [Online]. Available: https://www.researchgate.net/publication/240138198

[31] J. Garcia, R. Cerdeira, L. Coelho, P. Kumar, and M. da G. Carvalho, "Influence of Pedestrian Trajectories on School Children Exposure to PM $_{10}$," *J Nanomater*, vol. 2014, pp. 1–9, 2014, doi: 10.1155/2014/505649.

[32] J. N. P. M. Garcia *et al.*, "Analyses of human exposure to urban air quality in a children population," *Int J Environ Pollut*, vol. 40, no. 1/2/3, p. 94, 2010, doi: 10.1504/IJEP.2010.030886.

[33] S. Munir and T. M. Habeebullah, "Vehicular emissions on main roads in Makkah, Saudi Arabia—a dispersion modelling study," *Arabian Journal of Geosciences*, vol. 11, no. 18, p. 531, Sep. 2018, doi: 10.1007/s12517-018-3857-z.

[34] I. Petrou, K. Psistaki, I. M. Dokas, and A. K. Paschalidou, "Modelling the atmospheric dispersion of ammonia in an industrial area in northern Greece," *IOP Conf Ser Earth Environ Sci*, vol. 1123, no. 1, p. 012075, Dec. 2022, doi: 10.1088/1755-1315/1123/1/012075.

[35] O. Hertel, R. Berkowicz, and S. Larssen, "The Operational Street Pollution Model (OSPM)," in *Air Pollution Modeling and Its Application VIII*, Boston, MA: Springer US, 1991, pp. 741–750. doi: 10.1007/978-1-4615-3720-5_86.

[36] S. Di Sabatino, E. Solazzo, P. Paradisi, and R. Britter, "A Simple Model for Spatially-averaged Wind Profiles Within and Above an Urban Canopy," *Boundary Layer Meteorol*, vol. 127, no. 1, pp. 131–151, Apr. 2008, doi: 10.1007/s10546-007-9250-1.

[37] S. Awasthi and K. K. Chaudhry, "Numerical simulation and wind tunnel studies of pollution dispersion in an isolated street canyon," *Int J Environ Waste Manag*, vol. 4, no. 1/2, p. 243, 2009, doi: 10.1504/IJEWM.2009.026895.

[38] H. Greim, "Diesel Engine Emissions," in *Patty's Toxicology*, Wiley, 2023, pp. 1–8. doi: 10.1002/0471125474.tox129.

[39] P. Whitaker, P. Kapus, M. Ogris, and P. Hollerer, "Measures to Reduce Particulate Emissions from Gasoline DI engines," *SAE Int J Engines*, vol. 4, no. 1, pp. 2011-01–1219, Apr. 2011, doi: 10.4271/2011-01-1219.

[40] T. S. Wirawan, A. E. Eka Putra, and N. Aziz, "Gasoline Engine Performance, Emissions, Vibration and Noise with Methanol-Gasoline Fuel Blends," *IOP Conf Ser Earth Environ Sci*, vol. 927, no. 1, p. 012027, Dec. 2021, doi: 10.1088/1755-1315/927/1/012027.

[41] C. Zhong *et al.*, "Characteristics of Vehicle Tire and Road Wear Particles' Size Distribution and Influencing Factors Examined via Laboratory Test," *Atmosphere (Basel)*, vol. 15, no. 4, p. 423, Mar. 2024, doi: 10.3390/atmos15040423.

Edelweiss Applied Science and Technology
ISSN: 2576-8484
Vol. 8, No. 4: 881-899, 2024
DOI: 10.55214/25768484.v8i4.1468